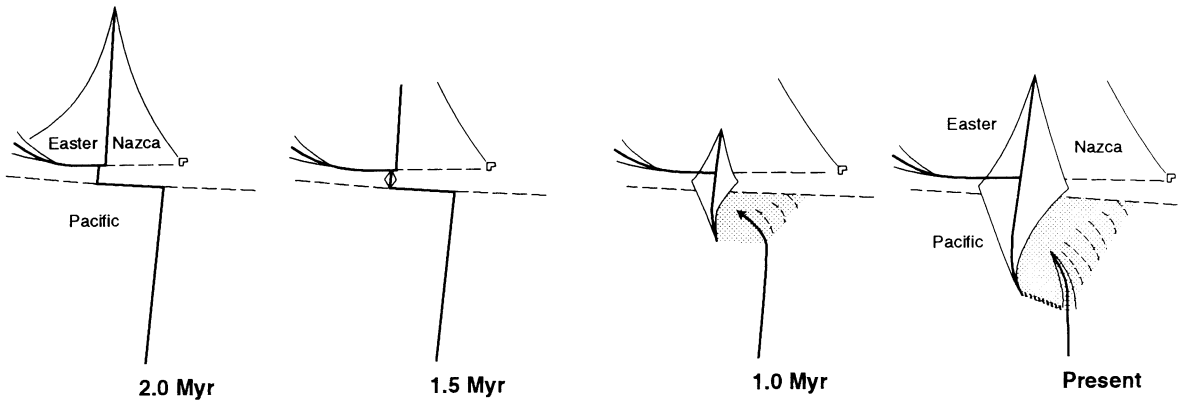

FIG. 4 Schematic evolution from transform fault to duelling propagators to possible proto-microplate. Heavy lines are active plate boundaries, long dashed lines are fracture zones, short dashed lines are failed rifts. Light lines are V-shaped pseudofault wakes of dominant propagators, arrows show briefly active duelling propagators. The northward propagator with outer pseudofault extending to Easter Island, shown schematically at 2 Myr (from ref. 3), is the one which seems to have initiated Easter microplate formation[1–3], probably driven by the magma pulse that formed Easter Island. Shading shows transferred lithosphere. Details of this evolution will be presented elsewhere (J.K. and R.N.H., manuscript in preparation).

microplate, the 120-km diameter requires[7] a rotation rate of 72° per Myr to match the regional spreading rates. The close fit of observed and predicted structures based on the propagating rift equations thus indicates at most a very brief period of additional microplate rotation. However, there are notable differences between the fossil and present overlap zones. No analogue of the NNW-trending rift graben, the northwest-trending scarp to the east, or the transform-like southern boundary in the present overlap zone is observed in the fossil overlap zone. This suggests that the tectonic behaviour has changed recently. One possibility is that a new microplate may be beginning to form here. A small rift graben adjacent to a transform boundary is also seen within the proposed Wilkes "nannoplate"[31], although grabens in migrating extensional relay zones have also been proposed to be characteristic of propagating rift systems[32].

Although there may have been a recent brief attempt to begin to rotate as a mostly rigid microplate, the successful evolution of this duelling propagator system into an edge-driven microplate[7] would require the eventual formation of a northern boundary as well. The width of this overlap zone (~120 km) is slightly smaller than those of the pervasively deformed cores of the Easter[2] and Juan Fernandez[5] microplates (~130–140 km), suggesting that this is about the scale at which pervasive sea-floor shearing of the overlap zone is no longer possible, the lithosphere stops deforming and begins to rotate as a rigid microplate[3,6,7,9,18]. The aspect ratios of the deformed cores of the microplates are ~3:1 (Easter) and ~2:1 (Juan Fernandez), suggesting that for this overlap zone to evolve into a similar microplate there would have to be a linkage event resulting from very rapid propagation that would double or triple the overlap length. □

Received 4 May; accepted 25 September 1995.

1. Hey, R. N. *et al. Nature* **317,** 320–325 (1985).
2. Searle, R. C. *et al. Nature* **341,** 701–705 (1989).
3. Naar, D. F. & Hey, R. N. *J. geophys. Res.* **96,** 7961–7993 (1991).
4. Francheteau, J., Yelles-Chaouche, A. & Craig, H. *Earth planet. Sci. Lett.* **86,** 253–268 (1987).
5. Larson, R. L. *et al. Nature* **356,** 571–576 (1992).
6. Searle, R. C., Bird, R. T., Rusby, R. I. & Naar, D. F. *J. geol. Soc. Lond.* **150,** 965–976 (1993).
7. Schouten, H., Klitgord, K. D. & Gallo, D. G. *J. geophys. Res.* **98,** 6689–6701 (1993).
8. Gallo, D. G. & Fox, P. J. (abstr.) *Eos* **63,** 446 (1982).
9. Engeln, J. F. & Stein, S. *Earth planet. Sci. Lett.* **68,** 259–270 (1984).
10. Bird, R. T. & Naar, D. F. *Geology* **22,** 987–990 (1994).
11. Hey, R. N. *Earth planet. Sci. Lett.* **37,** 321–325 (1977).
12. Schilling, J.-G., Sigurdsson, H., Davis, A. N. & Hey, R. N. *Nature* **317,** 325–331 (1985).
13. Hey, R. N., Duennebier, F. K. & Morgan, W. J. *J. geophys. Res.* **85,** 3647–3658 (1980).
14. McKenzie, D. P. *Earth planet. Sci. Lett.* **77,** 176–186 (1986).
15. Cormier, M.-H. & Macdonald, K. C. *J. geophys. Res.* **99,** 543–564 (1994).
16. Naar, D. F. & Hey, R. N. in *Evolution of Mid Ocean Ridges* (ed. Sinton, J. M.) 9–30 (American Geophysical Union, Washington DC, 1989).
17. Shackleton, N. J., Berger, A. & Peltier, W. R. *Trans. R. Soc. Edinb.* **81,** 251–261 (1990).
18. Klaus, A., Icay, W., Naar, D. F. & Hey, R. N. *J. geophys. Res.* **96,** 9985–9998 (1991).
19. Johnson, H. P. *et al. J. geophys. Res.* **88,** 2297–2315 (1983).
20. Macdonald, K. C., Haymon, R. M., Miller, S. P., Sempere, J.-C. & Fox, P. J. *J. geophys. Res.* **93,** 2875–2898 (1988).
21. Lonsdale, P. *J. geophys. Res.* **84,** 713–743 (1989).
22. Wilson, D. S. *Earth planet. Sci. Lett.* **96,** 384–392 (1990).
23. Kleinrock, M. C. & Hey, R. N. *J. geophys. Res.* **94,** 13859–13878 (1989).
24. Wetzel, L. R., Wiens, D. A. & Kleinrock, M. C. *Nature* **362,** 235–237 (1989).
25. Korenaga, J. *J. geophys. Res.* **100,** 365–378 (1995).
26. Hey, R. N., Kleinrock, M. C., Miller, S. P., Atwater, T. M. & Searle, R. C. *J. geophys. Res.* **91,** 3369–3393 (1986).
27. Phipps Morgan, J. & Parmentier, E. M. *J. geophys. Res.* **90,** 8603–8612 (1985).
28. Naar, D. F. & Hey, R. N. *Geology* **17,** 420–422 (1989).
29. Smith, W. H. F. & Sandwell, D. T. *J. geophys. Res.* **99,** 21803–21824 (1994).
30. Scheirer, D. S. & Macdonald, K. C. *J. geophys. Res.* **98,** 7871–7885 (1993).
31. Goff, J. A., Fornari, D. J., Cochran, J. R., Keeley, C. & Malinverno, A. *Geology* **21,** 623–626 (1993).
32. Kleinrock, M. C., Searle, R. C. & Hey, R. N. *J. geophys. Res.* **94,** 13839–13858 (1989).

ACKNOWLEDGEMENTS. We thank the captain and crew of the RV *Melville*, and J. Campbell and R. Beale of the GLORIA group for their help, the USGS for the use of their GLORIA/B system, and the government of Chile for permission to survey. We thank D. Wilson and J. Goff for reviews, D. McKenzie, R. Searle, J. Francheteau, B. Taylor, K. Macdonald, J. Phipps Morgan, P. Tapponnier, I. Manighetti and R. Armijo for discussions, and L. Norby, C. Inouye, T. Duennebier, and N. Hulbirt for assistance. This work was supported by the US NSF.

Elasticity of forsterite to 16 GPa and the composition of the upper mantle

Thomas S. Duffy*, Chang-sheng Zha, Robert T. Downs, Ho-kwang Mao & Russell J. Hemley

Geophysical Laboratory and Center for High-Pressure Research, Carnegie Institution of Washington, 5251 Broad Branch Road, NW, Washington DC 20015, USA

NEARLY 60 years ago, Bernal[1] proposed that a polymorphic phase transformation in olivine might be responsible for the seismic velocity discontinuity near 410 km depth in the mantle. Phase equilibria experiments[2,3] have since shown that the olivine (α) to wadsleyite (β) transition in $(Mg,Fe)_2SiO_4$ occurs at the appropriate pressure (13.8 GPa) under mantle conditions. Comparison of laboratory measurements of the acoustic velocity contrast in the α–β system to the magnitude of the seismically observed discontinuity at 410 km provides a way to constrain the olivine content of the mantle at this depth. Here we report measurements of the

* Present address: Consortium for Advanced Radiation Sources, The University of Chicago, 5640 South Ellis, Chicago, Illinois 60637, USA

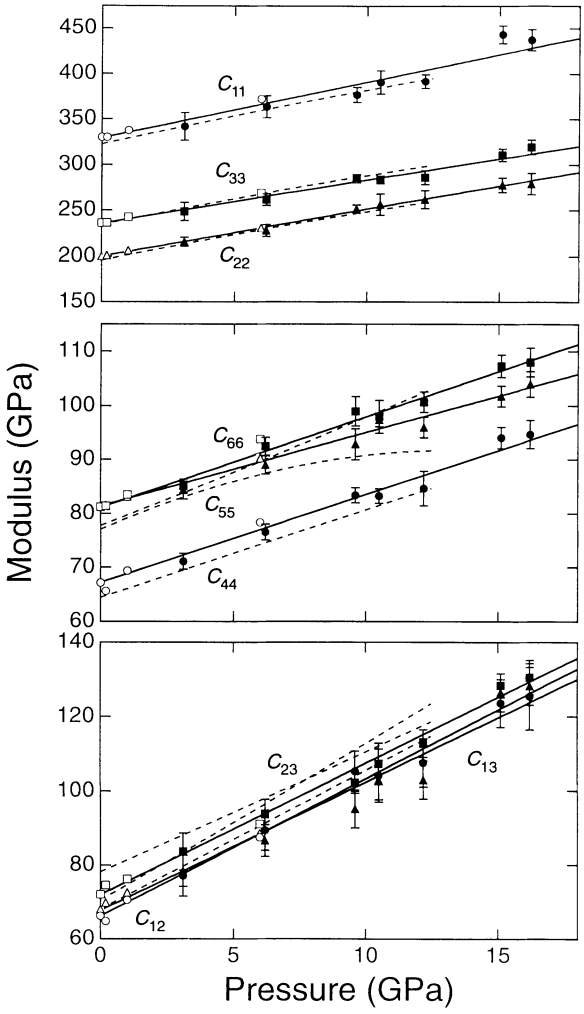

FIG. 1 Elastic moduli of single-crystal forsterite at 295 K as a function of pressure. Solid symbols with error bars (2σ) are present data. The root-mean-square misfit between the measured velocities and those calculated from the best-fitting elastic moduli is typically 0.6%. Additional scatter in the elastic moduli may arise from errors in measurement of pressure and scattering angle, correlations between fitted parameters, and non-hydrostatic stresses. Solid lines are least-squares fits to present results combined with ambient-pressure data[12]. The dashed lines are fits to ISS data[17] for $(Mg_{0.9}Fe_{0.1})_2SiO_4$. Open symbols show results of ultrasonic studies of Mg_2SiO_4 at the highest pressure attained in each experiment[4,5,15].

full set of elastic moduli of single-crystal forsterite (α-Mg_2SiO_4) at pressures between 3 and 16 GPa, using Brillouin scattering in a diamond anvil cell. At 13.8 GPa, the aggregate compressional- and shear-wave velocities of α-Mg_2SiO_4 are 2.7 ± 0.7% lower than predicted from earlier low-pressure data[4,5]. From our data, and assuming a homogeneous mantle composition, the seismic velocity contrast at 410 km depth can be satisfied only by a mantle containing less than ~40% olivine. This is well below the olivine abundance assumed in peridotite-based upper-mantle models.

The pyrolite model[2] of mantle composition is derived from the complementary melting relationships of basalts and peridotites, and contains ~60% olivine by volume. The primary uncertainty associated with this model is that it is derived from samples that originate from shallow depths (≤200 km) and assumes chemical homogeneity of the mantle as a whole. Compressional- (P) and shear-wave (S) seismic velocity profiles[6] provide the most direct constraints on the deep mantle. A number of studies[7-11] have addressed whether seismic data and laboratory measurements of acoustic wave velocities in $(Mg,Fe)_2SiO_4$ are consistent with a pyrolite mantle at 410 km depth, but have reached conflicting conclusions, in large part because of uncertainties in the relevant pressure and temperature dependences of the elastic moduli. Here our new measurements of the elasticity of α-Mg_2SiO_4 to transition-zone pressures are combined with other recent elasticity data[7,12,18] on the α–β system to constrain the amount of $(Mg,Fe)_2SiO_4$ consistent with laboratory and seismic data for the 410 km discontinuity.

Single crystals of synthetic forsterite were polished to flat plates ~20–60 μm thick in a plane intersecting the three crystal axes at nearly equal angles. Electron microprobe, polarizing microscopy, and X-ray diffraction confirmed that the samples were pure, unstrained single-crystal Mg_2SiO_4. The samples were loaded with ruby and a pressure-transmitting medium into a diamond anvil cell with 95° conical openings[19]. Pressures were determined by ruby fluorescence[20]. An argon pressure-transmitting medium was used at 3.1 and 6.1 GPa, a 4:1 methanol–ethanol mixture was used at 9.6 and 12.2 GPa, and helium was used at 10.5, 15.1 and 16.2 GPa, where the α-phase persists metastably at room temperature. Additional spectra were recorded at 9.6 GPa with a sample polished in the *b*–*c* plane. X-ray diffraction was carried out at each pressure to determine the crystal orientation and density, and to obtain information about the sample stress state[21].

Using Brillouin scattering, acoustic velocities can be determined from the frequency shift of light scattered from thermally generated acoustic waves. Brillouin spectra were recorded using an Ar^+ laser and a tandem Fabry–Perot interferometer[22]. The velocities of compressional and two shear acoustic waves were measured as a function of orientation at 10° intervals in a single plane at each pressure. The nine second-order elastic moduli of an orthorhombic crystal are related to acoustic velocities through Christoffel's equation[23]. The acoustic velocities were inverted using nonlinear least squares to obtain the elastic moduli as well as the three eulerian angles that specify the crystal orientation. The individual moduli were determined to a precision of 1–3% (1σ) and the crystal orientation is determined to ±2°. The orientation obtained from the Brillouin data is consistent with that determined by X-ray diffraction. Because of the lack of pure mode propagation directions, correlation coefficients between pairs of moduli could be significant. Monte Carlo simulations demonstrate that correlation errors largely cancel when computing aggregate properties.

The elastic moduli of forsterite at pressures between 3.1 and 16.2 GPa are shown in Fig. 1. All elastic moduli vary linearly with pressure within the resolution of our data. A recent study[17] used impulsive stimulated scattering (ISS) to measure the elastic moduli of $(Mg_{0.9}Fe_{0.1})_2SiO_4$ to 12.5 GPa in the diamond cell. The differences between our results and that study can be plausibly attributed to differences in sample iron contents. The most significant difference is that we find that C_{55} remains linear to 16.2 GPa in contrast to the nonlinear behaviour reported in ref. 17. The reason for this is not understood at present, but has no effect on the main conclusions of this study.

To date, models for upper-mantle mineralogy[8-11] have used very-low-pressure ultrasonic data[4,5] (to ≤1 GPa) extrapolated to higher pressures for comparison to seismic data. The pressure derivatives of the moduli determined here are uniformly lower

TABLE 1 Elastic properties of $(Mg_{0.9}, Fe_{0.1})_2SiO_4$

Property	α-phase	β-phase
K_S (GPa)	129 (1)*	174 (1)†
G (GPa)	79 (1)*	110 (1)†
$(\partial K_S/\partial P)_T$	4.2 (2)	4.8 (2)‡
$(\partial G/\partial P)_T$	1.4 (1)	1.7 (1)‡
$(\partial K_S/\partial T)_P$ (GPa K^{-1})	−0.017 (1)*	−0.018 (3)§
$(\partial G/\partial T)_P$ (GPa K^{-1})	−0.014 (1)*	−0.014 to −0.024

* Refs 12, 14; † ref. 26; ‡ ref. 7; § refs 16, 18.

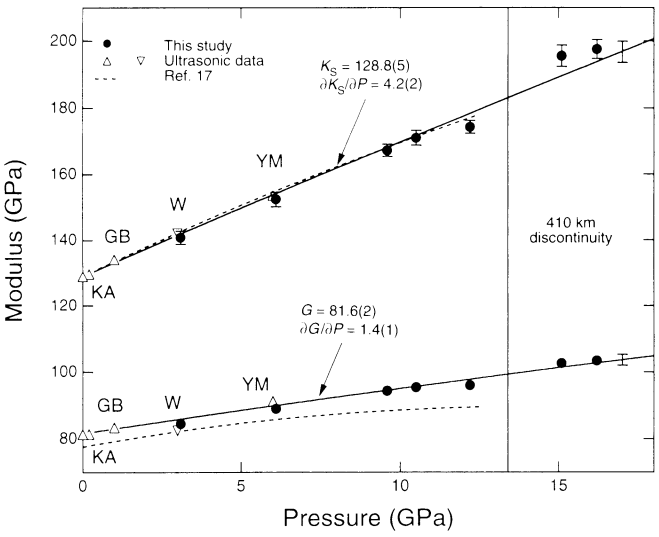

FIG. 2 Aggregate bulk and shear moduli of forsterite as a function of pressure. The solid symbols are data of this study, and solid lines are obtained from third-order finite strain fits to the data. Error bars represent the Voigt and Reuss limits[24] of the calculated aggregate moduli and are approximately the size of the symbols for the shear modulus. Confidence limits (1σ) on the fitted curve are shown by the error bar at 17 GPa. Dashed lines are from ISS data[17] for $(Mg_{0.9}Fe_{0.1})_2SiO_4$. Open symbols are from single-crystal ultrasonic studies of forsterite, with symbols shown at the highest pressure achieved in each experiment (KA[4], GB[5], YM[15]). The inverted triangle (labelled W) shows 3-GPa ultrasonic results[13] for $(Mg_{0.9}Fe_{0.1})_2SiO_4$. Vertical line shows the pressure of the 410 km seismic discontinuity.

than those of the low-pressure data by 30 ± 10% (ref. 4) and 20 ± 10%. (ref. 5) Systematic errors in, for example, pressure calibration are a possible explanation for the higher pressure derivatives measured in those studies.

The aggregate bulk modulus (K_S) and shear modulus (G) were calculated at each pressure from the average of the Voigt and Reuss bounds, which are limiting values of the moduli of a random, polycrystalline aggregate obtainable from single-crystal elasticity data[24] (Fig. 2). Fitting the data to finite strain expressions[25] yields values of 4.2 ± 0.2 and 1.4 ± 0.1 for the pressure derivatives of the adiabatic bulk and shear modulus, respectively (Table 1). The bulk and shear moduli, together with the density, define the compressional- and shear-wave velocities of a random polycrystalline aggregate. At 13.8 GPa, the aggregate velocities measured here are 2.7 ± 0.7% below those predicted from extrapolation of the previous data at 1 GPa or lower[4,5]. Our results are in good agreement, however, with recent forsterite data[15] to 6 GPa. For the bulk modulus, our results agree with data on Fe-bearing samples to 3 GPa (ref. 13) and 12.5 GPa (ref. 17). The pressure derivative of the bulk modulus determined from the Brillouin data is consistent with that determined solely from X-ray diffraction[21].

At ambient pressure and temperature, the P- and S-wave velocity contrasts between the α- and β-phases of Mg_2SiO_4 are[26] ~13%. One-dimensional seismic velocity profiles of the upper mantle constructed from analysis of body waves at both long and short periods yield velocity contrasts near 410 km that are generally in the range of 4–5% for compressional waves and 4–4.6% for shear waves[6,27–29]. The amount of forsterite consistent with the magnitude of the discontinuity is only 30–40% by volume, if the α–β velocity contrast is independent of pressure and temperature.

We next consider how the application of pressure affects the velocity contrast between the two phases. Ultrasonic measurements of acoustic velocities in a polycrystalline aggregate of β-Mg_2SiO_4 to 3 GPa have recently been reported[7]. Using pressure derivatives obtained from those measurements (Table 1) together with 1 GPa ultrasonic data for the α-phase[4], it was previously concluded that the α–β velocity contrast decreases significantly with pressure (at room temperature)[7]. But when our new values for the elasticity of the α-phase are used in this analysis, the velocity contrast is found to be nearly unchanged from ambient values (12% for P waves and 14% for S waves) at 13.8 GPa. Thus, the velocity contrast between the α- and β-phases of Mg_2SiO_4 is largely independent of pressure at ambient temperature.

We must then consider the combined effects of pressure and temperature on the α–β velocity contrast. This is done using a procedure outlined previously[10] and the parameters of Table 1. The densities and moduli are corrected for the effect of temperature and extrapolated adiabatically using third-order finite strain theory[25]. The elastic moduli are taken to be linear functions of temperature[12,14] and are corrected for the effect of 10 mol% Fe.

Recently, new measurements of the temperature sensitivity of the elastic moduli of the α-phase[12,14] and the isothermal bulk modulus of the β-phase[16,18], have been reported. These indicate that the temperature sensitivity of the bulk modulus is similar across the phase transition. The only parameter which has not been measured is the temperature dependence of the shear modulus, $\partial G/\partial T$, for the β-phase. We consider two possible values of this parameter. Measured values of $\partial G/\partial T$ for 15 silicates[30] fall in a range of −0.08 to −0.014 GPa K^{-1}. We adopt $\partial G/\partial T = -0.014$ GPa K^{-1} as a plausible estimate of $\partial G/\partial T$ for β-$(Mg_{0.9},Fe_{0.1})_2SiO_4$, identical to its value for the α-phase. Of the $\partial G/\partial T$ values reported for ~80 alkali halides, oxides and silicates[30], only a few are larger than −0.02 GPa K^{-1} in magnitude, and the largest reported value is −0.024 GPa K^{-1} (for MgO). We adopt this value as an upper-bound estimate of $\partial G/\partial T$ for β-Mg_2SiO_4.

Sound velocities in the $(Mg,Fe)_2SiO_4$ system along a 1,250 °C adiabat are shown in Fig. 3, together with seismic velocity profiles. The acoustic velocity jump in the α–β system far exceeds that observed in the seismic data when $\partial G/\partial T$ is constant across the transition. The fraction of olivine corresponding to the magnitude of the seismic discontinuity is 27% for shear waves, and 32% for compressional waves, assuming seismic velocity discontinuities of 4.3% and 4.5%, respectively. Although subject to potential systematic biases, the velocity jump in bulk sound velocity can be estimated by differencing P- and S-wave velocity

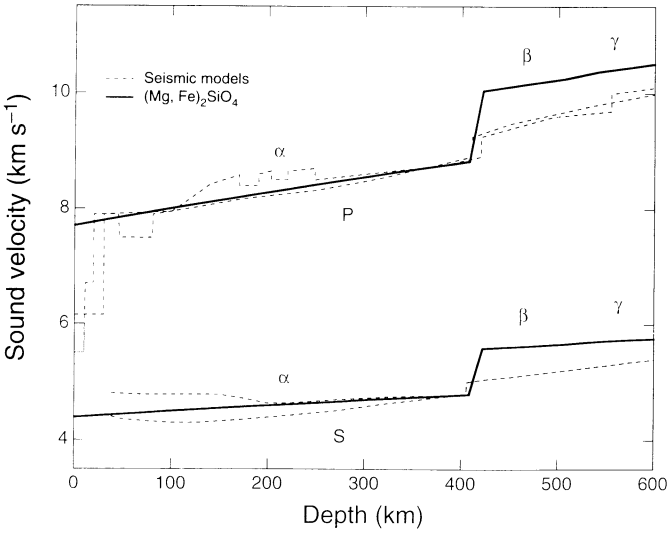

FIG. 3 Sound velocities in $(Mg_{0.9}Fe_{0.1})_2SiO_4$ along a 1,250 °C adiabat compared with seismic velocity profiles[27–29] for the upper mantle. The solid curve was calculated using $\partial G/\partial T = -0.014$ GPa K^{-1} for the β-phase, consistent with α-phase values. Also included are calculated acoustic velocities in the spinel (γ) phase of $(Mg,Fe)_2SiO_4$, which is stable below ~540 km depth.

profiles. The olivine abundance necessary to satisfy this data is 38%. Allowing the aggregate elastic moduli to vary within the Voigt and Reuss limits changes the calculated divine content by at most ± 5%.

When the larger value of $\partial G/\partial T$ is used in the calculation, the shear (and to a lesser extent, the compressional) wave velocities in the β-phase are reduced, due to increased temperature sensitivity. The fraction of olivine consistent with seismic data in this case becomes 44% for S waves and 40% for P waves, while remaining at 38% for bulk wave velocity. Thus, even assuming the rigidity of the β-phase is extremely temperature sensitive, current elasticity data for the $(Mg,Fe)_2SiO_4$ system are not consistent with an olivine-rich composition at 410 km depth.

Our approach assumes that the α–β phase change in a homogeneous mantle composition is the sole cause of the discontinuity. This simplification ignores effects of other possible phase transitions, and changes in element partitioning and the proportions of other phases across the transition. Phase equilibria data[31] suggest the last two effects can be neglected to first order. The first effect would only further reduce the amount of olivine required. It is also assumed that there is no texturing of the mineral aggregate, which, if present in the mantle at this depth, could significantly influence our results. The velocity anisotropy of forsterite at 15 GPa remains comparable to ambient-pressure values: 26% for P waves and 21% for S waves. If the pressure derivatives of the β-phase are much lower than present-day measurements suggest, the allowed olivine content of the mantle could be larger. For example, if $\partial K_S/\partial P$ and $\partial G/\partial P$ of the β-phase are assumed to be equivalent to α-phase values (4.2 and 1.4, respectively), the allowed mantle olivine content increases to ~52% (for $\partial G/\partial T = -0.024$ GPa K^{-1}). Future studies need to focus on developing a better understanding of the seismic structure of the 410 km discontinuity, as well as characterization of the elasticity of β-Mg_2SiO_4 to higher pressures and temperatures than yet achieved. □

Received 29 June; accepted 25 September 1995.

1. Bernal, J. D. *The Observatory* **59,** 268 (1936).
2. Ringwood, A. E. *Composition and Petrology of the Earth's Mantle* (McGraw-Hill, New York, 1975).
3. Akaogi, M., Ito, E. & Navrotsky, A. *J. geophys. Res.* **94,** 15671–15685 (1989).
4. Kumazawa, M. & Anderson, O. L. *J. geophys. Res.* **74,** 5961–5972 (1969).
5. Graham, E. K. & Barsch, G. R. *J. geophys. Res.* **74,** 5949–5959 (1969).
6. Nolet, G., Grand, S. P. & Kennett, B. L. N. *J. geophys. Res.* **99,** 23753–23766 (1994).
7. Gwanmesia, G. D., Rigden, S., Jackson, I. & Liebermann, R. C. *Science* **250,** 794–797 (1990).
8. Weidner, D. J. *Geophys. Res. Lett.* **12,** 417–420 (1985).
9. Bina, C. R. & Wood, B. J. *Nature* **324,** 449–451 (1986).
10. Duffy, T. S. & Anderson, D. L. *J. geophys. Res.* **94,** 1895–1912 (1989).
11. Ita, J. & Stixrude, L. *J. geophys. Res.* **97,** 6849–6866 (1992).
12. Isaak, D. G., Anderson, O. L. & Goto, T. *J. geophys. Res.* **94,** 5895–5906 (1989).
13. Webb, S. L. *Phys. Chem. Miner.* **16,** 684–692 (1989).
14. Isaak, D. G. *J. geophys. Res.* **97,** 1871–1885 (1992).
15. Yoneda, A. & Morioka, M. in *High-Pressure Research: Applications to Earth and Planetary Sciences* (eds Syono, Y. & Manghnani, M. H.) 207–214 (Terra Scientific, Tokyo, 1992).
16. Fei, Y. *et al. J. geophys. Res.* **97,** 4489–4495 (1992).
17. Zaug, J. M., Abramson, E. H., Brown, J. M. & Slutsky, L. J. *Science* **260,** 1487–1490 (1993).
18. Meng, Y. *et al. J. geophys. Res.* **98,** 22199–22208 (1993).
19. Mao, H. K. & Bell, P. M. *Yb. Carnegie Instn Wash.* **79,** 409–411 (1980).
20. Mao, H. K., Xu, J. & Bell, P. M. *J. geophys. Res.* **91,** 4673–4676 (1986).
21. Downs, R. T., Zha, C. S., Duffy, T. S. & Finger, L. W. *Am. Miner.* (in the press).
22. Zha, C. S., Duffy, T. S., Mao, H. K. & Hemley, R. J. *Phys. Rev.* B**48,** 9246–9255 (1993).
23. Every, A. G. *Phys. Rev.* B**22,** 1746–1760 (1980).
24. Watt, J. P., Davies, G. F. & O'Connell, R. J. *Rev. Geophys. Space Phys.* **14,** 541–563 (1976).
25. Davies, G. F. & Dziewonski, A. M. *Phys. Earth planet. Inter.* **10,** 336–343 (1975).
26. Sawamoto, H., Weidner, D. J., Sasaki, S. & Kumazawa, M. *Science* **224,** 749–751 (1984).
27. Grand, S. P. & Helmberger, D. V. *Geophys. J. R. astr. Soc.* **76,** 399–438 (1984).
28. Walck, M. C. *Geophys. J. R. astr. Soc* **76,** 697–723 (1984).
29. Mechie, J. *et al. Earth planet. Inter.* **79,** 269–286 (1993).
30. Sumino, Y. & Anderson, O. L. in *Handbook of Physical Properties of Rocks* Vol. III (ed. Carmichael, R. S.) 39–137 (CRC, Boca Raton, FL, 1989).
31. Akaogi, M. & Akimoto, S. *Phys. Earth planet. Inter.* **19,** 31–51 (1979).

ACKNOWLEDGEMENTS. We thank Hatten S. Yoder Jr for providing sample material and J. Ita for comments. This research was supported by the US NSF.

Preferential predation of female butterflies and the evolution of batesian mimicry

Naota Ohsaki

Entomological Laboratory, Faculty of Agriculture, Kyoto University, Kyoto, 606 Japan

BATESIAN mimicry, in which a palatable mimic resembles an unpalatable model, functions to protect insect mimics from birds. In butterflies that show batesian mimicry, female-limited mimicry is common[1–3]. The orthodox theory to explain this is sexual selection against males[4–6]. In these theoretical arguments, no difference in predation pressure between the sexes was assumed, but the existence of female-biased predation would enhance the evolution of sex-limited mimicry. To test for differences in attack rate between the sexes, I examined the rates of beak marks on wings of palatable butterflies of Papilionidae and Pieridae, and unpalatable Danaidae. Here I report that females were attacked more frequently than males, though danaids were generally attacked less. The papilionid and pierid males had low attack rates similar to those of danaid females. Analysis of a mathematical model highlighted these tendencies. Comparing a batesian mimetic species and its 'model' species, non-mimetic females were selectively attacked and the males, mimetic females and 'models' were attacked less. Therefore females benefit greatly when they become mimetic, whereas males will benefit much less should they become mimetic. Thus female-limited mimicry will be favoured even if the costs of mimicry to both sexes are the same.

In many cases of batesian mimicry, it is the females that are mimetic whereas the males are non-mimetic. There has been no established theory to explain the evolution of female-limited mimicry, although more than 1,500 papers on mimicry have been published this century[3]. The orthodox theory is that mimicry tends to be limited to females in butterflies as a result of sexual selection against males. However, there is a classic but slighted hypothesis that non-mimetic females are selectively

TABLE 1 Percentage of butterflies with beak marks on wings

	Large damage (%)*		Damage including small (%)		Number of captured individuals		
	Males	Females	Males	Females	Males	Females	Females/Males
Papilionidae	28.1	43.4	39.8	54.7	231	53	0.23
Pieridae	23.9	35.9	41.1	55.0	331	120	0.36
Danaidae	14.7	23.2	22.6	35.4	190	99	0.52

Papilionidae, Pieridae and Danaidae include 17, 15 and 17 species, respectively. The genera *Troides* and *Trogonoptera* of Papilionidae and genus *Delias* of Pieridae, most species of which are supposed to be unpalatable, are not included. Therefore, all species of Papilionidae and Pieridae are probably palatable and all species of Danaidae are unpalatable.

* Large marks (≥5 mm) were inflicted only by bird attacks in cage experiments, whereas small marks (<5 mm) were inflicted not only by bird attacks but also by some obstacles such as branches[12].